Published in final edited form as:
Nat Ecol Evol. ; 1: . doi:10.1038/s41559-017-0083.

Sulfate radicals enable a non-enzymatic Krebs cycle precursor

Markus A. Keller[1,2,3], **Domen Kampjut**[1], **Stuart A. Harrison**[1], and **Markus Ralser**[1,4]

[1]Department of Biochemistry and Cambridge Systems Biology Centre, University of Cambridge, 80 Tennis Court Rd, Cambridge CB2 1GA, UK

[2]Division of Biological Chemistry, Biocenter, Medical University of Innsbruck, Innrain 80-82, 6020 Innsbruck, Austria

[3]Division of Human Genetics, Medical University of Innsbruck, Peter-Mayr-Straße 1, 6020 Innsbruck, Austria

[4]The Molecular Biology of Metabolism Laboratory, The Francis Crick Institute, 1 Midland Rd, NW1 1AT, London, UK

Abstract

The evolutionary origins of the tricarboxylic acid cycle (TCA), or Krebs cycle, are so far unclear. Despite a few years ago, the existence of a simple non-enzymatic Krebs-cycle catalyst has been dismissed ‘as an appeal to magic’, citrate and other intermediates have meanwhile been discovered on a carbonaceous meteorite and do interconvert non-enzymatically. To identify the non-enzymatic Krebs cycle catalyst, we used combinatorial, quantitative high-throughput metabolomics to systematically screen iron and sulfate reaction milieus that orient on Archean sediment constituents. TCA cycle intermediates are found stable in water and in the presence of most iron and sulfate species, including simple iron-sulfate minerals. However, we report that TCA intermediates undergo 24 interconversion reactions in the presence of sulfate radicals that form from peroxydisulfate. The non-enzymatic reactions critically cover a topology as present in the Krebs cycle, the glyoxylate shunt and the succinic semialdehyde pathways. Assembled in a chemical network, the reactions achieve more than ninety percent carbon recovery. Our results show that a non-enzymatic precursor for the Krebs cycle is biologically sensible, efficient, and forms spontaneously in the presence of sulfate radicals.

Introduction

The tricarboxylic acid cycle (TCA), or Krebs cycle, is a central metabolic pathway typically of oxidative function. This metabolic pathway provides precursors for the biosynthesis of

To whom correspondence should be addressed: Markus Ralser, Tel +44 1223 761346, markus.ralser@crick.ac.uk.

Author Contributions

M.A.K. and M.R. designed the research; M.A.K., D.K. and S.A.H. performed the research; M.A.K and M.R. wrote the first draft of the paper, and all authors contributed to finalizing the manuscript.

Competing financial interests

The authors declare no competing financial interest.

Europe PMC Funders Author Manuscripts

amino acids, is central to fatty acid breakdown, cellular respiration, energy and redox metabolism1. The widespread occurrence of at least its oxidative part2,3 indicates that the origins of at least parts of the Krebs cycle are to be placed to a very early stage in evolution, perhaps its oxidative reactions date back to origin of life4–6. A frequently discussed hypothesis proposes the Krebs cycle obtained its structural topology by Darwinian selection principles that were enabled by the 'RNA world'. A post-genetic origin implies that pathway topologies are subject to progressive change, implying that the modern Krebs cycle could differ substantially from its early precursors7. A post-genetic origin of metabolism struggles however to explain how multiple, structurally complex enzymes came into being initially; enzymes themselves are made-up from the metabolic products of the Krebs cycle. Second, a Darwinian origin of the metabolic network topology has difficulties to explain the high number of reactions that are recurring between kingdoms despite a lack of enzyme sequence conservation8. An alternative hypothesis hence proposes that at least the key metabolic reactions originated from an environmental chemistry. In this scenario, the inorganic catalysis determine the basic structure of metabolism9–12.

As enzymatic mechanisms of the Krebs cycle have limited resemblance to inorganic catalysis, a non-enzymatic origin was received skeptically by many5,13. For instance, Leslie Orgel, a leading scientist in shaping the RNA world hypothesis, dismissed the possibility that a simple inorganic catalyst that could replace a series set of TCA-like reactions as 'an appeal to magic'5. However, despite the simple catalyst was indeed missing so far, others have argued that several Krebs-cycle metabolites form in organic-chemical reactions9,10. Meanwhile, the presence of a series TCA intermediates has been confirmed on a carbonaceous meteorite 14. Furthermore, citrate and other TCA intermediates undergo highly efficient reductive, interconversion reactions on semiconductor particles upon strong UV light exposure15. A non-enzymatic precursor to the Krebs cycle is hence catalytically possible. Moreover, also the existence of an unifying, simple catalyst has become plausible. Non-enzymatic reactions that replicate two other metabolic pathways, glycolysis the pentose phosphate pathway, are unified by their dependency on the same catalyst and co-substrate, ferrous iron16,17. As Fe(II) is abundant in typical Archean sediments18,19 implies that the general chemical environments, rather than niche conditions, could have been key to shape the structure of metabolic pathways.

We choose a systematic screening strategy and addressed in ~4,850 absolute quantitative experiments the reactivity of TCA intermediates in the presence of typical Archean sediment constituents as well as related iron and sulfur species. We find TCA intermediates unreactive in the presence of the majority of iron and sulfate combinations, including the simple FeS mineral ferrous sulfide. In the presence of the radical donor peroxydisulfate however, we detect 24 non-enzymatic interconversion reactions. These reactions resemble the isomerisation and oxidative reactions of the enzymatic Krebs cycle, the glyoxylate shunt and the succinic semialdehyde pathway, so that their topologies are critically covered. A chemical network assembled from these reactions achieves more than 90% carbon recovery, forming a plausible non-enzymatic template for the origin of the early Krebs cycle.

Results

We optimized the throughput of a liquid chromatography-multiple reaction monitoring (LC-MRM) method to absolutely quantify TCA intermediates in the 6,100 samples eventually created in this study. We next assessed the reactivity of citrate, cis-aconitate, isocitrate, α-ketoglutarate, succinate, fumarate, malate and oxaloacetate upon heat exposure in water and - and in order to account for the low oxygen concentrations of the pre-metabolic world20 - in an artificial nitrogen atmosphere. TCA intermediates were stable and did not react spontaneously into other TCA intermediates or other products (Figure 1AB, Supplementary Figure 1). The only exception was oxaloacetate that decarboxylated forming pyruvate (Figure 1B, Supplementary Figure 2). The Krebs cycle hence contrasts to glycolysis and pentose phosphate pathways, of which intermediates spontaneously interconvert16,17. Non-enzymatic TCA-like reactivity is hence highly depending on enabling chemistry. Further, these experiments served as important controls as they confirm the absence of enzymatic contamination.

Transition metals are prebiotically abundant and remain frequent metabolic catalysts 21. We tested a transition metal mixture that reflects iron, cobalt, nickel and molybdenum concentrations of typical Archean sediments18,19,22 and found that isocitrate reacted to α-ketoglutarate, succinate and pyruvate, and α-ketoglutarate to succinate (Figure 1C, Supplementary Table 1). These reactions were dependent Fe(II) (Supplementary Figure 3, Supplementary Table 2), and hence likely dependent on the α-hydroxyl or α-keto moieties specifically present in isocitrate and α-ketoglutarate that form iron contact sites (Figure 1D)23. Furthermore, these reactions followed a clear pH-profile (Supplementary Figure 4), similar to Fe(II) mediated glycolysis-like reactions17.

The low number of reactions ruled out the transition metal catalysis is sufficient to enable a non-enzymatic Krebs cycle (Figure 1D). A major bottleneck where the conversions of citrate to isocitrate and succinate to fumarate, typically catalyzed by iron-sulfur cluster enzymes24. Iron/sulfur minerals such as pyrite could have acted as catalysts in a prebiotic metabolism4, but mineral surfaces chemistry has little resemblance to metabolic catalysis either. We tested ferrous sulfide as a simple mimetic of an iron sulfur mineral, but detected no TCA-like reactions (Supplementary Tables 3-4 and Supplementary Figures 5-6). We continued with a systematic screen, testing ten sulfur-containing compounds, seven iron sources, and five TCA substrates in all possible combinations (Figure 2A). Again, most reaction mixtures had no effect on TCA intermediates (Figure 2B). However, a comprehensive spectrum of reactivity was enabled upon adding peroxydisulfate (Figure 2B, Supplementary Table 3). In the single-timepoint screening format, we detected up to 13 TCA-metabolite forming reactions (Figure 2B, Supplementary Figures 5-6).

We noticed that when combined with iron sources, in particular ferrous sulfide, the reaction spectrum enabled by peroxydisulphate was substantially altered. Most reactions were accelerated, while some intermediates were no longer observed at the expense of additional TCA metabolites that were formed (Supplementary Table 1). We hence continued with a detailed and quantitative (kinetic) characterization of the reactions starting from citrate, cis-aconitate, isocitrate, α-ketoglutarate, succinate, succinic semialdehyde, fumarate, and malate

in the presence of peroxydisulphate in combination with ferrous sulfide. In the quantitative time series analyses, we detected 24 reactions that interconvert a TCA metabolite into another TCA intermediate (Fig 3A). A network graph assembled from these reactions reveals a high coverage of the topologies of the TCA cycle (by resembling its oxidative and isomerisation reactions), the glyoxylate shunt and the succinic semialdehyde pathways (Figure 3B-C).

Considering that our conditions were optimized to obtain a maximum number of TCA-like reactions, but not yield, the TCA-like chemical network was found extraordinarily efficient. After 2 h, 91.9% of the carbon was recovered in TCA intermediates, of which 42.3% were newly formed TCA metabolites. Only 8.1% reacted into non-TCA metabolites (including carbon dioxide) (Figure 3C).

The 24 non-enzymatic reactions did occur at an average rate of 0.280 μmol per min starting from the 100 μM substrates in the presence of peroxydisulphate and ferrous sulfide, but solely at 0.0433 μmol per min in the absence of ferrous sulfide. The interconversion of succinic semialdehyde to succinate was the fastest, and the reaction of citrate to succinate was the slowest reaction (Fig 3A, Supplementary Figure 7). Also the two reactions enabled by Fe(II) (Figure 1), were substantially faster in the peroxydisulfate/ferrous sulfide milieu, and did occur at 33.0% or 34.7%, of the Fe(II) rate (Figure S7, Supplementary Table 1). Further, the intermediates that were exclusively detected in the presence of peroxydisulphate, are likely exclusive to the simple milieu as they react faster to the downstream product than they are formed once the iron sources are combined with peroxydisulfate (Fig 3A). Peroxydisulfate can act via a radical one-electron and a two-electron mechanism25 and possesses a high oxidative potential26,27 which results from the donation of sulfate radicals, increasingly formed upon activation by iron and iron-containing sediments including pyrite28, other trace metals29,30, as well as by photolysis and thermolysis31,32. Implying that the TCA-like reactions are dependent on the formation of these radicals, we assessed the effects of hydrogen peroxide (H_2O_2), that in the presence of Fe(II), provides hydroxyl radicals in the Fenton reaction. 10 out of the 24 reactions were enabled also by H_2O_2 (Figure 4A, Supplementary Table 5). The specificity was however 83% lower and the reactions 91.1% slower (Figure 4A). Next, we exploited the differential scavenging properties of 2-propanol and tert-butanol. While 2-propanol efficiently scavenges both, hydroxyl and sulfate radicals ($k_{(OH^{\bullet})}$ = 1.9*109 M-1s-1, $k_{(SO_4^{-\bullet})}$ = 8.2*107 M-1s-1), tert-butanol inefficiently scavenges the sulfate radical ($k_{(SO_4^{-\bullet})}$ = 8.5*105 M-1s-1, compared to the hydroxyl radical ($k_{(OH^{\bullet})}$= $5.2*10^8$ $M^{-1}s^{-1}$) (Figure 4B, left panel)33. *tert*-butanol did not prevent TCA-like reactions, but scavenging of sulfate radicals by 2-propanol abolished most reactivity (Figure 4B, C, Supplementary Table 5). Radical quenching had lower impact on some reactions, which could be explained by incomplete scavenging or by non-radicalic activity of peroxydisulfate and its product (Figure 4D). For the majority of reactions, the presence of sulfate radicals was however essential.

Discussion

All living cells possess a metabolic network whose topological structure is conserved between kingdoms, also for pathways like glycolysis and its variants where the enzymes are

not sequence conserved. Sometimes confused with another important question about whether life was of heterotrophic or autotrophic origin34, the origin of this metabolic network remains a largely unsolved problem35–37. An increasing number of experiments reveal that its core structural parts are resemblant of spontaneous chemical reactions and non-enzymatic catalysis16,21,38A theory that explains the metabolic origin by an environmental inorganic chemistry is indeed attractive, as it facilitates a stepwise scenario for origin of enzymes39,40. In the presence of a chemical network not all enzymes that form pathway need to come into being at the same time to achieve a functional unit41. Second, a chemical system can be improved stepwise starting from its single most limiting reaction.

Fe(II) dependent on-enzymatic reactions that resemble glycolysis and the pentose phosphate pathway16,17 reveal that metabolism-like reaction networks can form on the basis of a simple and prebiotically abundant catalyst. Seen from another perspective, chemical reactions that are driven by the most abundant Archean transition metal are part of the metabolic network. Several key questions remain however unanswered. First, there is currently no prebiotically plausible scenario that forms the glycolytic and PPP precursors such as glucose-6-phosphate or 6-phosphogluconate, respectively. Further, it remains that glycolytic and PPP-like reactions cannot serve to explain the origin of other pathways that depend on a different chemistry, like the Krebs cycle, that does not possess phosphorylated intermediates.

Attractive about the Krebs cycle is that the non-enzymatic formation of its intermediates has has repeatedly been described, including their presence in high concentrations on a carbonaceous meteorite13–15. In the systematic search for a plausible Krebs-cycle catalyst, we excluded chemical conditions that can not persist within the boundaries of a cell (in particular UV light, high pressure, temperatures above 100°C), avoided niche conditions and metals that play virtually no role in metabolism (i.e. titan, borate). Instead, we screened metals important for metabolism that are frequent Archean sediment components, use low-oxygen conditions, and compromise on a temperature (70°C) that enables to measure slow reactions, yet that is within the range of life.

While TCA cycle intermediates were highly stable, our HTP screen revealed a single hit. Peroxydisulfate enabled a series of TCA-like reactivity, and we find that this property was dependent on the formation of sulfate radicals. The non-enzymatic reactions obtained reflect the oxidative and isomerisation reactivity of the Krebs cycle, the glyoxylate shunt and the succinic semialdehyde pathways (Fig 2) and form a chemical reaction network was of extraordinary high yield of > 90%. Indeed in several reactions the formation of non-TCA metabolites was negligible (Fig 3C). In other words, TCA metabolites interconvert specifically into TCA intermediates under the elaborated conditions, but barely form any other of the many thermodynamically possible products. To put this into perspective, the yield of the non-enzymatic network exceeds substantially that of an *in vitro* glycolysis based on *E. coli* purified enzymes 42. An explanation for this high specificity is provided by the physical-chemical properties of the sulfate radical. Compared to hydroxyl radicals with a half-life time of only 10^{-9} sec in water, sulfate radicals are orders of magnitude more stable, and persist for several seconds43. Furthermore, the sulfate radical carries a negative charge at physiological pH, and thus is affected by a repulsive force between itself and the

substrates charged carboxyl groups. These electrostatic interactions limit the approachable reactive positions of TCA intermediates. In addition, the spatial dimensions of sulfate radicals create a steric burden that decreases the number of possible contact sides. All these properties limit the number of contact sites and reaction products, that are found the intermediates of the Krebs cycle, at least its stable end products of multi-step reactions as observed in our set-up (Supplementary Table 6). The reactions observed include decarboxylations, oxidoreductase like redox reactions, and dehydrations, and for some a reaction topology like in the TCA cycle is obtained. For instance, succinate is formed from citrate, aconitate, isocitrate, and α-ketoglutarate. These reactions show a similar dependency on sulfate radicals and a comparable quenching behaviour, This implies that succinate is formed in a reaction sequence that starts with citrate forming cis-aconitate, which is then converted to isocitrate, α-ketoglutarate, succinic semialdehyde and finally succinate. In contrast, the formation of pyruvate from citrate appears independent from radical species, while other pyruvate forming reactions are quenched by the radical scavenger. Pyruvate is hence formed by more than one reaction.

The dependency of almost all reactions on sulfate radicals could be indicative about the prebiotic environment in which the Krebs cycle emerged. Despite the reactive radicals themselves are not be preserved over billions of years, there are indirect traces of an early sulfur redox chemistry. Microfossils in 3.4-billion-year-old rocks of Western Australia are some of the earliest traces of life on Earth, and are characterized by pyrite microfossils of biotic origin44. This difference to glycolysis and the PPP, that depend on Fe(II) but not on sulfur species16. This observation might add an aspect to the endosymbiont theory. While glycolysis and the PPP are typically cytoplasmic, in most eukaryotic species that contain mitochondria, these are both the host of the TCA cycle and are responsible for the assembly of iron-sulfate clusters 45.

How could a series of non-enzymatic reaction enable the evolution of the Krebs ‘cycle’, that does not only interconvert and oxidize metabolites, but is is also implicated in anabolism and that contains key co-factor coupled reactions? To complete the Krebs cycle, a C-C forming reaction to yield citrate as catalyzed by citrate synthase is required but missing. However a full or reductive cycle is present only in a subset of species, and hence unlikely the evolutionary starting point for the Krebs cycle2,3. Indeed, an oxidative directionality is the expected thermodynamic outcome for non-enzymatic reactions. Cofactor-dependent reactions reverse the directionality in living systems, and these are considered a speciality of enzymatic catalysis. The closure of the TCA cycle by adding a citrate synthase enzyme could r provide a significant advantage upon adding a single enzymatic step, and hence provide an interesting case for the evolution of an enzyme-catalysed metabolism. One possibility hence consists that first versions of the Krebs cycle could have been of heterotrophic nature that obtained precursors from environmental-chemical reactions that do not necessarily need to possess resemblances with metabolic pathways14,15. Alternatively, we would like to speculate that there is also no need for an early closure of the Krebs cycle, if its oxidative reactions are fed by other metabolism-like reactions, like a carboxylation of pyruvate enabled in a coupling to an early glycolysis. The existence of non-enzymatic pyruvate carboxylase reaction latter could unify key issues of explaining the origins of glycolysis, the PPP and the Krebs cycle.

Europe PMC Funders Author Manuscripts

In summary, we describe a mutually compatible, efficient, non-enzymatic catalysis that interconverts TCA cycle intermediates. The reactions are enabled by sulfate radicals that form upon the activation of peroxydisulfate. The chemical network coves the topology of the conserved (oxidative) part of the Krebs cycle, and achieves more than 90% carbon efficiency. The simplicity of the environment that is based on a unifying catalyst, reveals that the Krebs cycle could have hence emerged from a non-enzymatic precursor that forms spontaneously in the presence of sulfate radicals.

Methods

General Study Design

Sample size—Experiments exploring the available chemical reaction space are constrained by combinatorics: the number of samples multiplies with each additional condition to be tested. To address this issue, we simplified and optimized sample preparation, LC-SRM measurement and statistical analysis for screening purposes at the expense of an exact rate determination. We then utilized more resource consuming methods for optimal chromatographic separation and absolute quantification of reaction rates in all subsequent verification experiments. This allowed us to measure a total of more than 4,850 samples along with 1,250 controls, external standards and blanks and to efficiently analyse and manually curate the corresponding ~65,000 LC-SRM chromatograms as specified below.

Replicates and time series—Each calculated reaction rate is based on a time series experiment with six collection points, which were performed in at least three replicates. Reaction rate was calculated only for those reactions that showed a significant product accumulation over time that was consistent in all three replicates. Consequently, for rate calculation of one reaction under a certain condition a total of 18 measurement points were used.

Sample collection / endpoints—Sampling points in time course experiments were typically set to 0, 10, 30, 60, 120 and 300 min in order to cover both relatively fast and slow reactions. The reaction oxaloacetate -> pyruvate was the only reaction which was too fast for these timescales and we designed an alternative experimental setup with narrower time windows to follow this reaction.

Quality control and Outliers—Peaks were identified by matching retention time and fragmentation properties to externally measured chemically pure standards. Automated peak picking and integration of specific transitions by MassHunter (Agilent) was backed up by additional manual inspection of all peaks (see below). We controlled for cross-contaminations and carry-over by repeated measurement of blanks and substrate-free controls.

Materials

Metabolite standards were obtained at high purity. If not otherwise indicated, the product number refers to Sigma-Aldrich: sodium citrate (71635), sodium isocitrate (I1252), cis-

aconitic acid (A3412), sodium α-ketoglutarate (K2010), sodium succinate (14160), succinic semialdehyde (Santa Cruz Biotechnology, F1114), sodium fumarate (F1506), L-malic acid (M6413), sodium pyruvate (P2256), oxaloacetic acid (O4126), iron acetate (FeAc, 339199), $FeCl_2$ (372870), $FeCl_3$ (157740), $Fe(ClO_4)_2$ (334081), $Fe(ClO_4)_3$ (309281), ferrocene (F408), FeS(268704), H_3PO_4 (P5811), 2-mercaptoethanol (Merck Millipore, 805740), cysteine (30095), DL-ethionine (E5139), dimethylsulfoxid (D8418), homocysteic acid (69453), $NaHSO_3$ (Acros Organics, 41944), methionine (M9375), ammonium peroxydisulfate (Fischer Scientific, 10219790), sodium sulfite Na_2SO_3 (Fischer Scientific, 10070400), sodium sulfate Na_2SO_4 (Fischer Scientific, 10493372). All water was obtained commercially at UPLC-MS purity (Biosolve Chemicals, Cat no. 23214102).

LC-SRM method for TCA metabolite quantification

For quantification of TCA intermediates an Agilent 1290 Infinity Binary LC system with an online coupled Agilent 6460 Triple Quadrupole Mass Spectrometer was used. Sample separation was achieved on a Zorbax Eclipse Plus C18 Rapid Resolution column (1.8 um, 2.1 x 50 mm, Agilent, column temperature 30°C). Solvent A contained 5% methanol, 0.2% acetic acid, 10 mM tributylamine in UPLC grade water (Greyhound) and Solvent B was 100% methanol (Greyhound). 1.5 - 2.5 µl of sample were injected on the column at 0.5 ml/min followed by gradient elution as detailed in UPLC Gradient Supplementary Tables 7-11. Needle wash to prevent sample carryover was performed by water:acetonitrile (2:1) containing FlushPort wash with each injection. Including washing and re-equilibration this resulted in total cycle times between 4.4 (4.15) and 16 min, depending on the gradient. (see gradients S7-11).

Mass spectrometric quantification of specific products was performed in multiple or selective reaction monitoring (MRM or SRM) mode. Instrument parameters and metabolite transitions for each feature were optimized using pure commercially available standards (Supplementary Tables 12-13). MS/MS data were analyzed with Masshunter Workstation (Agilent) using QQQ Quantitative Analysis Software package. All automatically integrated peaks were manually curated in order to ensure high data quality and consistency with regularly measured quality control standards. Repeatedly measured external standard dilution series were used for determination of absolute metabolite concentrations. Further analysis and fitting of reaction rates was performed in R (R Core Team, http://www.R-project.org).

Data analysis - Rate determination

For each replicate the recorded time series was used to determine product formation rates (time dependent accumulation of reaction products). Different fitting algorithms were used to account for varying modes of product formation, caused by dissimilar chemical properties of substrate, product, and co-products and other effects such as intermediate stabilities, reaction orders or reaction induced changes of the chemical environment. The models used were i) a least squares linear model for continuous product formation, ii) the nonlinear growth model $y = a \cdot {}^{-b \cdot c}$ being part of the SSgompertz module in R, iii) the maximum initial growth rate within the linear range using the least squares model to be used for products with dynamic formation/degradation behaviour iv) and an exponential decay model

following the format $y = a \cdot 2^{(-b \cdot x)} + c$. The best fitting model was chosen according to the respective R^2 values and was confirmed by graphical, manual review of the plotted curves.

Data analysis - Statistical analysis of iron/sulfur reactivity screen

Differential raw peak area data ($\Delta X_i = X_{t=300} - X_{t=0}$) between t = 300 min and t = 0 min were calculated from the individual LC-SRM peak areas extracted using the Masshunter software (Agilent) and were indicative for an accumulation of products (positive values) or the deletion of substrates (negative values). Assuming normal distribution we then calculated z-scores (z_i) (for graphical representation see Supplementary Figure 5): $i = -\frac{median(X)}{\sigma(X)}$ with $\sigma(X)$ being approximated by the median absolute deviation (MAD) according to: $\sigma = MAD(X) \cdot 1.4826$. z-Scores were then converted into p-values using normal distribution function f(x) with $\mu = 0$ and $\sigma = 1$:

$$p - value = 2(for\ 2 - sided) \cdot f(x) = \frac{2}{\sqrt{2} \cdot \sigma} \cdot e^{\frac{|i|^2}{2}}$$

All calculations were done in R using standard inbuild functions including mad() and pnorm(). A graphical representation of the results can be found in Figure 2B and Supplementary Figure 6.

Iron-rich sediment simulation experiments

100 μM of each individual TCA substrate were combined with a freshly prepared metal rich mixture (200 μM $FeCl_2$, 10 nM $CoCl_2$, 400 nM $NiCl_2$, 10 nM MoO_4 and 100 μM H_3PO_4) in a low-oxygen N_2 atmosphere generated by three repeated vacuum/N_2 gas cycles in an anoxic chamber (Coy Lab Products, USA). The mixtures were then sealed in HPLC glass vials (5182-0717 and 5182-0716, Agilent) and incubated at 70°C in a water bath. For all substrates other than oxaloacetate samples were collected after 0, 10, 30, 60, 120, and 300 min by rapid cooling on ice. This resulted in measurement of 486 samples plus controls. After incubation the reaction mixtures were transferred to 384-well plates (Greiner Bio-One, 781186) under normoxic conditions and stored at -80°C for subsequent LC-SRM measurement using the UHPLC gradient in Supplementary Table 7.

Individual metal effect

In order to determine the contribution of individual metals towards facilitating specific TCA metabolite interconversions we tested each of the constituents of the Archean sediment simulation for their catalytic potential. The same experimental setup as above was applied, using isocitrate and α-ketoglutarate as substrates and mixing them with each metal individually (200 μM $FeCl_2$, 200 μM $FeCl_3$, 10 nM $CoCl_2$, 400 nM $NiCl_2$, 10 nM MoO_4, 100 μM H_3PO_4) under low-oxygen and in the case of Fe(III) normoxic conditions. Substrate and products in 324 sample plus controls were measured with the LC-SRM method using UHPLC gradient S8.

Reaction mixtures containing oxaloacetate were generated by combining oxaloacetate with $FeCl_2$ at the same concentrations as stated above but under normoxic conditions, directly

Europe PMC Funders Author Manuscripts

followed by incubation at 40°C in the autosampler of the Agilent 1290 HPLC system. Instead of stopping the reaction on ice the HPLC was programmed to automatically inject 1.5 µl of the sample onto the column every 5 min for up to 2.5 hrs. The three replicates for the $FeCl_2$ condition and the iron-free control were measured in alternating order. Substrates and products in 113 samples plus controls were measured with a LC-SRM method using the UHPLC gradient in Supplementary Table 8.

pH-dependency

In order to determine the effects of pH on ferrous iron induced non-enzymatic reactivity the interconversion experiments were carried out in the presence of 5 mM sodium phosphate buffering at pH points 3, 5, 6, 7, 8, and 9 in analogy to the experiments described in 17. Furthermore the reaction mixture consisted of 100 µM isocitrate (or water as control) and 200 µM iron(II) chloride (Sigma-Aldrich, 372870). The correct starting pH was controlled for by initial measurement, and kept constant throughout the incubations via the buffer capacity of the respective buffer. Substrates and products in 252 samples plus 56 controls were measured with a LC-SRM method using the UHPLC gradient in Supplementary Table 9.

Screening of iron/sulfur compounds for their catalytic impact on TCA cycle intermediates

For screening of iron and/or sulfur species that actively promote non-enzymatic reactivity among TCA metabolites the experimental setup was adapted to be performed in 96-well format. Samples were prepared in glass-coated 96 well plates (96 PLATE+ 7MM RD U 300UL PP, Thermo Scientific), sealed in low oxygen conditions and additionally vacuum-packed to prevent any possible well to well cross-contamination. 100 µM citrate, cis-aconitate, succinate, malate and fumarate were used as substrate individually and mixed with all possible combinations of 200 µM of different iron sources (FeAc, $FeCl_2$, $FeCl_3$, $Fe(ClO_4)_2$, $Fe(ClO_4)_3$, ferrocene, FeS and iron-free controls) and 200 µM of inorganic or organic sulfur species (2-mercaptoethanol, cysteine, DL-ethionine, dimethylsulfoxid, homocysteic acid, $NaHSO_3$, methionine, $(NH_4)_2S_2O_8$, Na_2SO_3, Na_2SO_4 and sulfur-free controls). The samples were heated to 70°C in a water bath for 0 and 300 min. This resulted in a total of 1320 samples plus controls. Samples were then transferred to 384-well plates (Greiner Bio-One, 781186) under normoxic conditions and stored at -80°C for subsequent LC-SRM measurement using the UHPLC gradient in Supplementary Table 10.

Non-enzymatic TCA qualitative and quantitative (kinetic) validation experiments

On the basis of the statistical analysis of the iron/sulfur screening results we selected the most potent non-enzymatic interconversion conditions and verified them in time series experiment with three replicates using a comprehensive targeted mass spectrometric quantification method. The substrates citrate, isocitrate, cis-aconitate, α-ketoglutarate, succinate, succinic semialdehyde, fumarate and malate were diluted to 100 µM in UPLC grade water and mixed with 200 µM peroxydisulfate in the presence of absence of 200 µM ferrous sulfide (FeS). In analogy to the experiments above these mixtures were sealed under anoxic conditions and were incubated at 70°C in a water bath. Samples were collected after 0, 10, 30, 60, 120 and 300 min by rapid cooling on ice, resulting in 432 samples plus

controls, which were transferred to 384 well plates and stored at -80°C for subsequent LC-SRM analysis using the UHPLC gradient in Supplementary Table 11.

Non-enzymatic TCA reactions: recovery and specificity calculations

Recovery rates were quantified via the quotient of the respective TCA metabolites at timepoint t=0 and the total sum of concentrations measured after 2 hours of incubation at 70°C. The fraction of products at timepoint t=2 hours compared to the total sum of TCA metabolites (substrate + products) was calculated to determine the percentage of specific TCA products. Please note, the absolute quantification of citrate in presence of peroxydisulfate (and with it the calculated recovery rate) is hampered by an unusually high variance (CV = 25.6%) for this metabolite due to an unknown 20 mechanism/ chemical interference (the average variance for all other features, metabolites, and recovery rates remains low (CV = 3.48%). For this technical reason, the recovery rate calculated for citrate and the efficiency of the reactions that start with citrate, have a higher uncertainty according to this CV value.

Comparison of hydrogen peroxide and peroxydisulfate as radical donors for non-enzymatic TCA-like reactivity

In order to investigate the potential contribution of sulfur radical species to the non-enzymatic reactivity facilitated by peroxydisulfate we compared them to hydroxyl radicals generated from hydrogen peroxide. In three replicates we incubated 100 μM citrate, isocitrate, cis-aconitate, alpha-ketoglutarate, succinate, fumarate and malate with 200 μM hydrogen peroxide or 200 μM peroxydisulfate at 70°C under anoxic conditions and collected samples after 0, 10, 30, 60, 120 and 300 min (378 samples plus controls) and measured them by LC-SRM analysis using the UHPLC gradient in Supplementary Table 11.

Sulfate and hydroxyl radical scavenging experiments

The differential radical scavenging properties of 2-propanol and *tert*-butanol were exploited to test for the importance of sulfate over hydroxyl radicals. In these experiment 200 μM peroxydisulfate was mixed with 100 μM citrate, isocitrate, cis-aconitate, α-ketoglutarate, succinate, fumarate or malate individually and each combination was treated with 500 μM 2-propanol, 500 μM *tert*-butanol or water as a control. Samples were sealed under anoxic conditions, heated to 70°C in a water bath and incubated for 0, 10, 30, 60, 120 and 300 min (504 samples plus controls) and then measured by LC-SRM analysis using the UHPLC gradient in Supplementary Table 11.

Data Availability

The reaction rate data is provided in the Supplementary Tables 1-5; the raw quantification data files have been deposited in the Mendeley Data repositroy (http://dx.doi.org/10.17632/vgpmnzdz55.1)

Supplementary Material

Refer to Web version on PubMed Central for supplementary material.

Acknowledgements

We thank George Averill and Timo Littmann for helping with experiments. This work was supported by the Francis Crick Institute which receives its core funding from Cancer Research UK (FC001134), the UK Medical Research Council (FC001134), and the Wellcome Trust (FC001134), the Wellcome Trust (RG 093735/Z/10/Z to MR), and the ERC (Starting grant 260809 to MR) for funding. MAK is supported by an Erwin Schrödinger postdoctoral fellowship (FWF, Austria, J3341). DK is supported by an Ad Futura studentship (Slovene Scholarship Fund).

References

1. Krebs HA, Johnson WA. The role of citric acid in intermediate metabolism in animal tissues. FEBS Lett. 1980; 117(Suppl):K1–10.
2. Huynen MA, Dandekar T, Bork P. Variation and evolution of the citric-acid cycle: a genomic perspective. Trends Microbiol. 1999; 7:281–291. [PubMed: 10390638]
3. Meléndez-Hevia E, Waddell TG, Cascante M. The puzzle of the Krebs citric acid cycle: assembling the pieces of chemically feasible reactions, and opportunism in the design of metabolic pathways during evolution. J Mol Evol. 1996; 43:293–303. [PubMed: 8703096]
4. Wachtershauser G. Evolution of the first metabolic cycles. Proceedings of the National Academy of Sciences. 1990; 87:200–204.
5. Orgel LE. Self-organizing biochemical cycles. Proc Natl Acad Sci U S A. 2000; 97:12503–12507. [PubMed: 11058157]
6. Sojo V, Herschy B, Whichler A, Camprubí E, Lane N. The Origin of Life in Alkaline Hydrothermal Vents. Astrobiology. 2016; 16:181–197. [PubMed: 26841066]
7. Hud NV, Cafferty BJ, Ramanarayanan K, Williams LD. The Origin of RNA and 'My Grandfather's Axe'. Chem Biol. 2013; 20:466–474. [PubMed: 23601635]
8. Brasen C, Esser D, Rauch B, Siebers B. Carbohydrate Metabolism in Archaea: Current Insights into Unusual Enzymes and Pathways and Their Regulation. Microbiol Mol Biol Rev. 2014; 78:89–175. [PubMed: 24600042]
9. Morowitz HJ, Kostelnik JD, Yang J, Cody GD. The origin of intermediary metabolism. Proceedings of the National Academy of Sciences. 2000; 97:7704–7708.
10. Smith E, Morowitz HJ. Universality in intermediary metabolism. Proceedings of the National Academy of Sciences. 2004; 101:13168–13173.
11. Brilli M, Fani R. Cellular Origin and Life in Extreme Habitats and Astrobiology. 2004:129–132.
12. Shapiro R. A Replicator Was Not Involved in the Origin of Life. IUBMB Life. 2000; 49:173–176. [PubMed: 10868906]
13. Zubarev DY, Rappoport D, Aspuru-Guzik A. Uncertainty of prebiotic scenarios: the case of the non-enzymatic reverse tricarboxylic acid cycle. Sci Rep. 2015; 5:8009. [PubMed: 25620471]
14. Cooper G, Reed C, Nguyen D, Carter M, Wang Y. Detection and formation scenario of citric acid, pyruvic acid, and other possible metabolism precursors in carbonaceous meteorites. Proc Natl Acad Sci U S A. 2011; 108:14015–14020. [PubMed: 21825143]
15. Zhang XV, Martin ST. Driving parts of Krebs cycle in reverse through mineral photochemistry. J Am Chem Soc. 2006; 128:16032–16033. [PubMed: 17165745]
16. Keller MA, Turchyn AV, Ralser M. Non-enzymatic glycolysis and pentose phosphate pathway-like reactions in a plausible Archean ocean. Mol Syst Biol. 2014; 10:725. [PubMed: 24771084]
17. Keller MA, et al. Conditional iron and pH-dependent activity of a non-enzymatic glycolysis and pentose phosphate pathway. Sci Adv. 2016; 2:e1501235. [PubMed: 26824074]
18. Rouxel OJ, Bekker A, Edwards KJ. Iron isotope constraints on the Archean and Paleoproterozoic ocean redox state. Science. 2005; 307:1088–1091. [PubMed: 15718467]
19. Saito MA, Sigman DM, Morel FMM. The bioinorganic chemistry of the ancient ocean: the co-evolution of cyanobacterial metal requirements and biogeochemical cycles at the Archean–Proterozoic boundary? Inorganica Chim Acta. 2003; 356:308–318.
20. Canfield DE, Habicht KS, Thamdrup B. The Archean sulfur cycle and the early history of atmospheric oxygen. Science. 2000; 288:658–661. [PubMed: 10784446]
21. Belmonte L, Mansy SS. Metal Catalysts and the Origin of Life. Elements. 2016; 12:413–418.

22. Zerkle AL. Biogeochemical signatures through time as inferred from whole microbial genomes. Am J Sci. 2005; 305:467–502.
23. Siegel B, B S, J L. Iron-catalyzed oxidative decarboxylation of benzoylformic acid. Journal of the American Chemical Society. 1979; 101:2221–2222.
24. Tong W-H, Rouault TA. Metabolic regulation of citrate and iron by aconitases: role of iron-sulfur cluster biogenesis. Biometals. 2007; 20:549–564. [PubMed: 17205209]
25. Kolthoff IM, Miller IK. The Chemistry of Persulfate. I. The Kinetics and Mechanism of the Decomposition of the Persulfate Ion in Aqueous Medium 1. J Am Chem Soc. 1951; 73:3055–3059.
26. Sra KS, Thomson NR, Barker JF. Persistence of persulfate in uncontaminated aquifer materials. Environ Sci Technol. 2010; 44:3098–3104. [PubMed: 20205387]
27. Peyton GR. The free-radical chemistry of persulfate-based total organic carbon analyzers. Mar Chem. 1993; 41:91–103.
28. Liang C, Chenju L, Yi-Yu G, Yi-Chi C, Yi-Jhen W. Oxidative Degradation of MTBE by Pyrite-Activated Persulfate: Proposed Reaction Pathways. Ind Eng Chem Res. 2010; 49:8858–8864.
29. Liang C, Bruell CJ, Marley MC, Sperry KL. Persulfate oxidation for in situ remediation of TCE. I. Activated by ferrous ion with and without a persulfate-thiosulfate redox couple. Chemosphere. 2004; 55:1213–1223. [PubMed: 15081762]
30. Teel AL, Ahmad M, Watts RJ. Persulfate activation by naturally occurring trace minerals. J Hazard Mater. 2011; 196:153–159. [PubMed: 21968122]
31. Herrmann H, Hartmut H. On the Photolysis of Simple Anions and Neutral Molecules as Sources of O-/OH, SOx- and Cl in Aqueous Solution. ChemInform. 2007; 38
32. Liang C, Chenju L, Bruell CJ. Thermally Activated Persulfate Oxidation of Trichloroethylene: Experimental Investigation of Reaction Orders. Ind Eng Chem Res. 2008; 47:2912–2918.
33. Ahmad M, et al. Oxidative and Reductive Pathways in Iron-Ethylenediaminetetraacetic Acid–Activated Persulfate Systems. J Environ Eng. 2012; 138:411–418.
34. Schönheit P, Wolfgang B, Martin WF. On the Origin of Heterotrophy. Trends Microbiol. 2016; 24:12–25. [PubMed: 26578093]
35. Bar-Even A, et al. The moderately efficient enzyme: evolutionary and physicochemical trends shaping enzyme parameters. Biochemistry. 2011; 50:4402–4410. [PubMed: 21506553]
36. Tawfik DS. Accuracy-rate tradeoffs: how do enzymes meet demands of selectivity and catalytic efficiency? Curr Opin Chem Biol. 2014; 21:73–80. [PubMed: 24954689]
37. Luisi PL. An open question on the origin of life: the first forms of metabolism. Chem Biodivers. 2012; 9:2635–2647. [PubMed: 23161640]
38. Laurino P, Tawfik DS. Spontaneous Emergence of S-Adenosylmethionine and the Evolution of Methylation. Angew Chem Int Ed Engl. 2017; 56:343–345. [PubMed: 27901309]
39. Ralser M. The RNA world and the origin of metabolic enzymes. Biochem Soc Trans. 2014; 42:985–988. [PubMed: 25109990]
40. Keller MA, Piedrafita G, Ralser M. The widespread role of non-enzymatic reactions in cellular metabolism. Curr Opin Biotechnol. 2015; 34:153–161. [PubMed: 25617827]
41. Horowitz NH. On the Evolution of Biochemical Syntheses. Proceedings of the National Academy of Sciences. 1945; 31:153–157.
42. Itoh A, et al. Application of capillary electrophoresis-mass spectrometry to synthetic in vitro glycolysis studies. Electrophoresis. 2004; 25:1996–2002. [PubMed: 15237399]
43. Sies H. Strategies of antioxidant defense. Eur J Biochem. 1993; 215:213–219. [PubMed: 7688300]
44. David W, Kilburn MR, Martin S, John C, Brasier MD. Microfossils of sulphur-metabolizing cells in 3.4-billion-year-old rocks of Western Australia. Nat Geosci. 2011; 4:698–702.
45. Lill R, Kispal G. Maturation of cellular Fe–S proteins: an essential function of mitochondria. Trends Biochem Sci. 2000; 25:352–356. [PubMed: 10916152]
46. Lill R, Kispal G. Maturation of cellular Fe–S proteins: an essential function of mitochondria. Trends Biochem Sci. 2000; 25:352–356. [PubMed: 10916152]

Europe PMC Funders Author Manuscripts

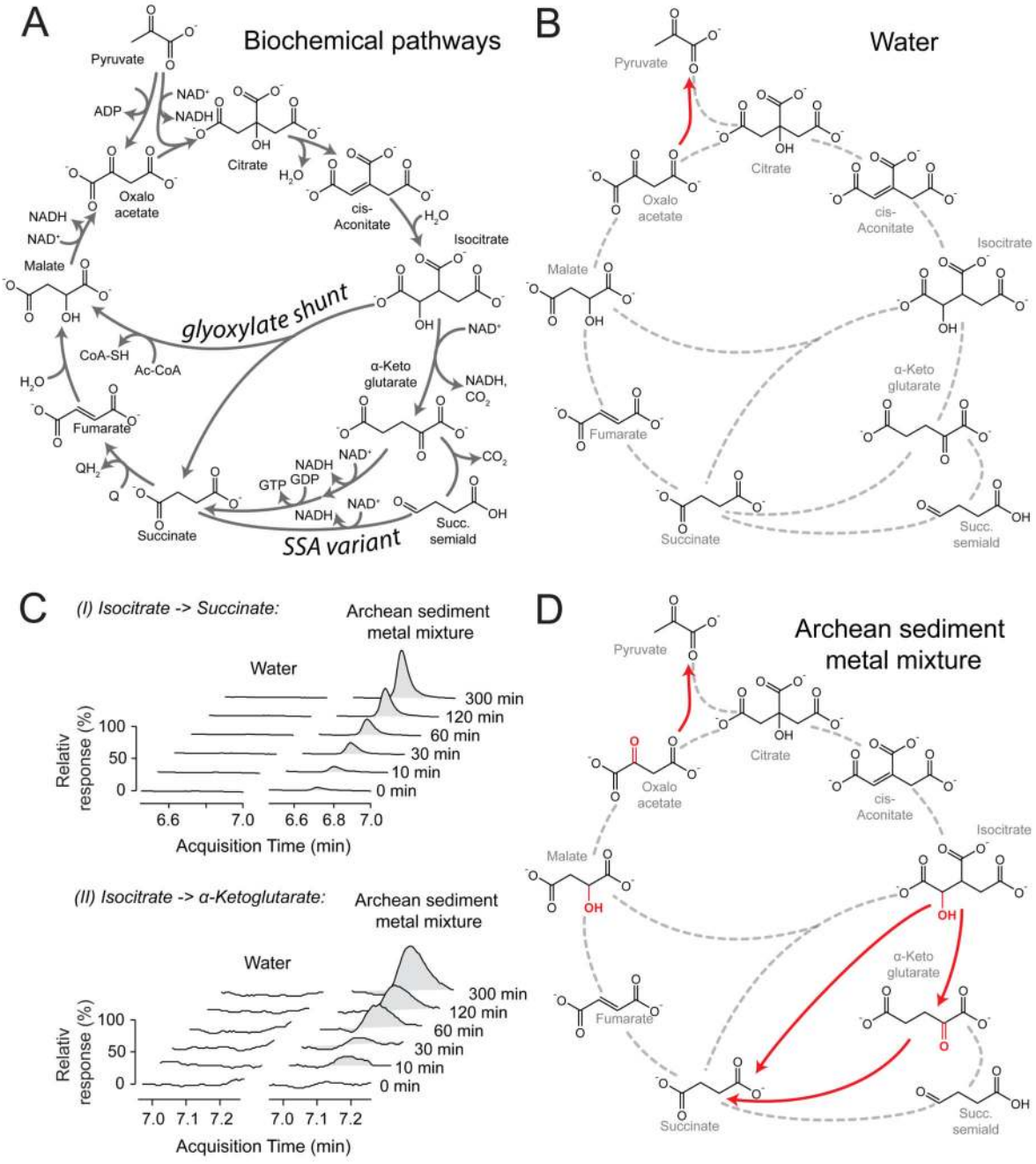

Figure 1. TCA intermediates are stable in water and show some reactivity in the presence transition metals frequent in Archean sediments.

A) Reaction scheme of the TCA cycle, including a canonical topology for the Krebs cycle the glyoxylate shunt and the succinic semialdehyde pathway. B) TCA intermediates are considerably stable in 70°C water; no reactivity is detected within 5 hours, except for oxaloacetate which forms pyruvate (Supplementary Figure 2). C) An Archean sediment-like transition metal mixture increases reactivity. Isocitrate forms α-ketoglutarate, succinate and pyruvate, while α-ketoglutarate forms succinate (Supplementary Figure 3).

D) Reactions as identified (C) projected to a TCA cycle graph. α-hydroxyl and α-keto moieties that allow specific interaction with ferrous iron are indicated in red.

Europe PMC Funders Author Manuscripts

Europe PMC Funders Author Manuscripts

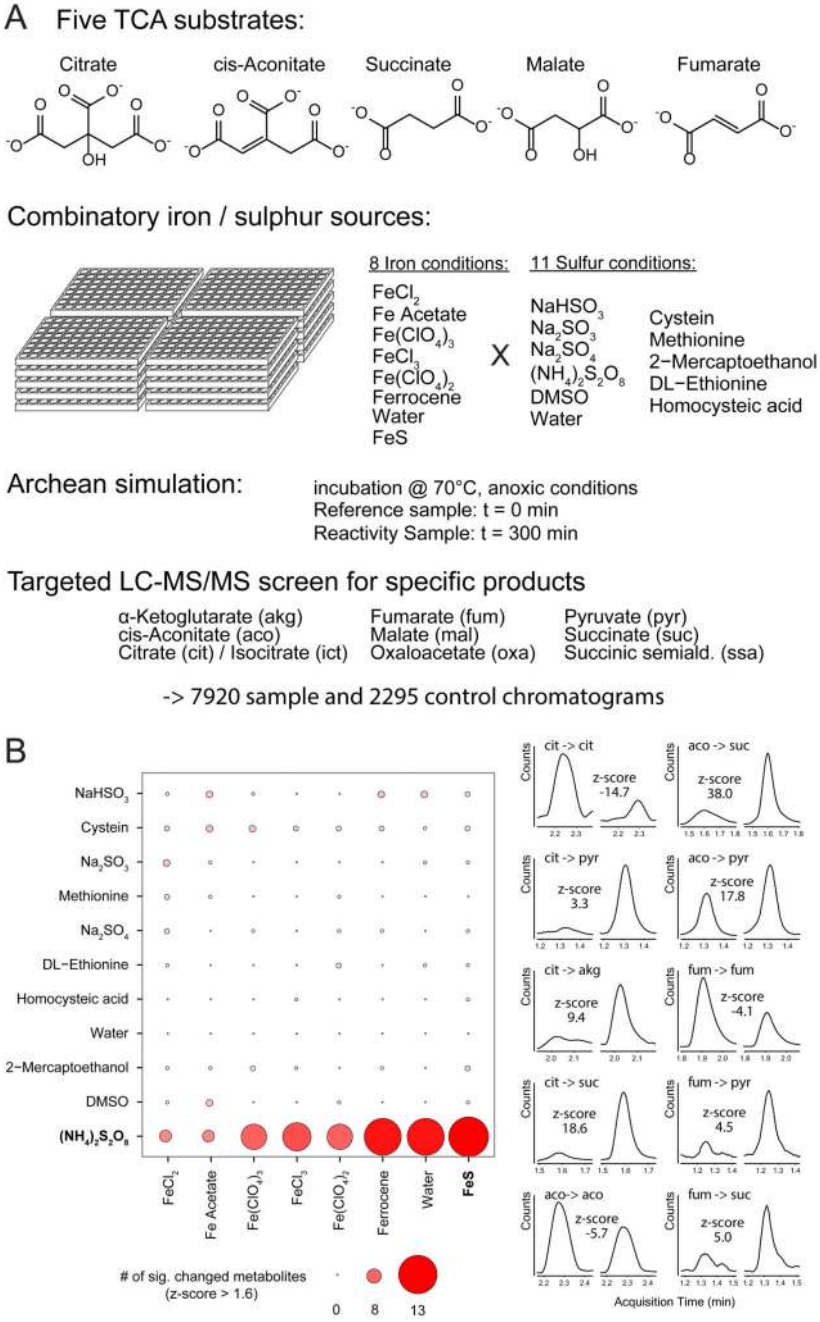

Figure 2. Peroxydisulfate enables the non-enzymatic interconversion of TCA intermediates.

A) Combinatorial condition screening: Five TCA intermediates were co-incubated for 0 and 300 min in combinations of eight iron and eleven sulfur sources. B) Significant reactions, expressed as c.p.s. illustrated in a heat matrix (left panel). For each possible reaction, product accumulation and substrate consumption over 300 min were calculated from integrated SRM signals. Most conditions did not reveal significant reactivity (significance threshold z > 1.6; Supplementary Table 3, Supplementary Figures 5-6). Right panel: Ten

examples of significant reactions as detected upon a combination of peroxydisulfate with ferrous sulfide. left: 0 min, right: 300 min.

Europe PMC Funders Author Manuscripts

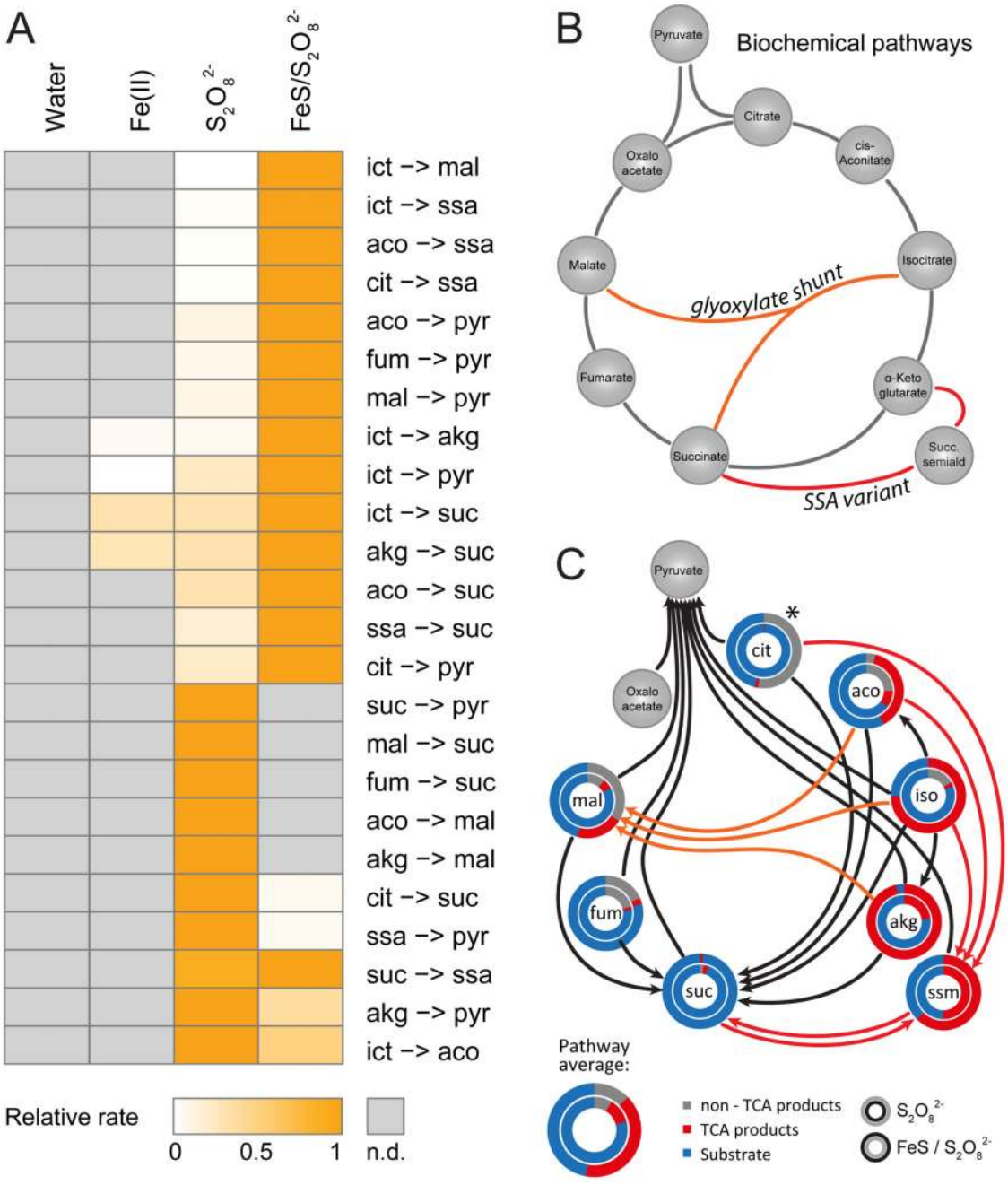

Figure 3. Non-enzymatic Krebs-cycle like reactions in the presence of peroxydisulfate and peroxydisulfate/ferrous sulfide.

A) Non-enzymatic TCA reactivity (relative reaction rates, normalized so that they can be compared) in the presence of peroxydisulfate and/or ferrous sulfide. Not detected (n.d.) reactions are depicted in grey (Supplementary Table 4 and Supplementary Figure 7 for rate data). B) Schematic illustration of the enzyme-catalysed Krebs cycle (black), glyoxylate shunt (orange), and succinic semialdehyde pathway (red). C) Non-enzymatic TCA-like reactions are highly efficient and replicate large parts of the reaction spectrum of the TCA cycle, the glyoxylate shunt and the succinic semialdehyde pathways. Non-enzymatic

reactions were coloured according to whether they replicate the Krebs cycle (black), the glyoxylate shunt (orange), or the succinic semialdehyde route (red), as in (B). Circle diagrams illustrate the efficiency, expressed as TCA metabolite recovery as substrate (blue), newly formed TCA intermediate (red), or carbon loss (grey) indicative of the formation of non-TCA intermediates. The inner circles reflect peroxydisulfate, the outer circles the combination of peroxydisulfate and ferrous sulfide. Please note that for citrate quantifications have a higher technical variability in the combination of peroxydisulfate and ferrous sulfide, see Methods for details.

Europe PMC Funders Author Manuscripts

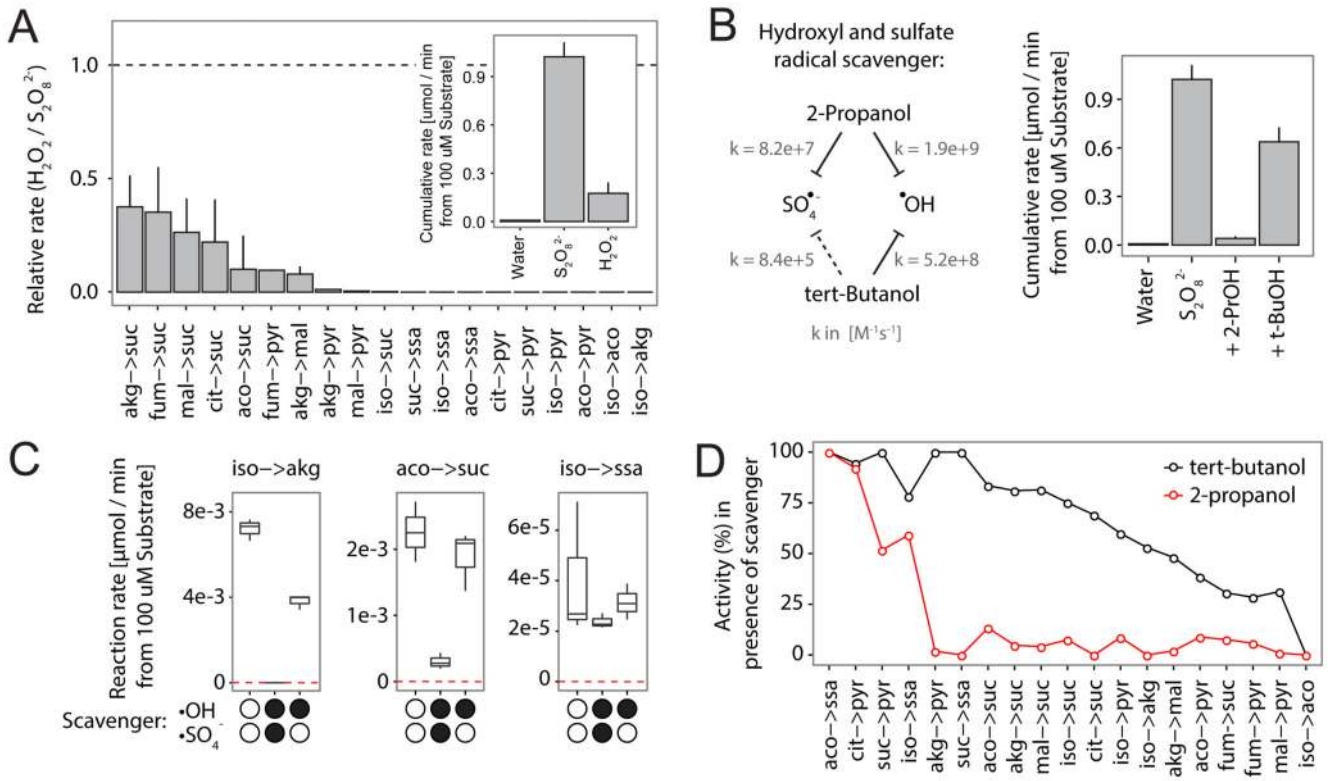

Figure 4. Peroxydisulfate enables TCA-like reactivity by providing sulfate radicals.

A) Comparison of sulfate and hydroxyl radical donors on TCA-like non-enzymatic reactions. Reaction rates were determined in the presence of hydrogen peroxide (H_2O_2) and are given relative to the respective rate in the presence of peroxydisulfate ($(NH_4)S_2O_8$). H_2O_2 enables a subset of reactions that are in average 91.1% slower. Insert: Total absolute cumulative reactivity comparing hydrogen peroxide, peroxydisulfate and control (water). Data is given as mean ± SD, n=3. B) Left panel: Differential scavenging capacities of 2-propanol and *tert*-butanol allow discriminating between reactivity mediated by sulfate or hydroxyl radicals. Right panel: The reactivity mediated by peroxydisulfate is quenched by the sulfate radical scavenger. Data is given as mean ± SD, n=3 (Supplementary Table 5 for rate data). C) The effects of 2-propanol and *tert*-butanol on three representative non-enzymatic reactions (black dots represent the presence of a particular scavenger). For the reaction isocitrate to α-ketoglutarate a strong effect of 2-propanol and a medium effect of *tert*-butanol was measured. The reactions *cis*-aconitate -> succinate and isocitrate -> succinic semialdehyde were mainly, but to different completion, affected by the sulfate radical scavenger. D) Differential scavenger effects of 2-propanol (red) and *tert*-butanol (black) confirm the reaction dependency on sulfate radicals. Values were calculated on basis of the ability of scavengers to reduce non-enzymatic reactivity compared to controls as described in (C).

Europe PMC Funders Author Manuscripts